Communication

Mutual Coupling Compensation for Compact MIMO Radar

Zhou Jianxiong, Zhu Rongqiang, and Li Haorun

***Abstract*— A calibration method to compensate for the mutual coupling and channel imbalance in a compact multi-input multi-output (MIMO) radar array based on turn table measurements is proposed. Two mutual coupling matrices, one for the transmit array and the other for the receive array, are used to model the relationship between the ideal manifold and the measured manifold. The practical factors such as the nonisotropic element pattern and the displacement of the array phase center are also taken into account. All the unknowns are determined by solving the nonlinear least-squares fitting problem iteratively. Using two coupling matrices consists of the mutual coupling mechanism in an MIMO array and has better calibration performance than using one matrix for the virtual array. It also reduces the dimension of the matrix and hence the computation load of calibration. Measurements by a microstrip array with two transmitters and four receivers are used to verify its effectiveness in angle estimation, beamforming, and superresolution of close targets.**

***Index Terms*— Array calibration, compact multi-input multi-output (MIMO) radar, mutual coupling.**

I. Introduction

Compact multi-input multi-output (MIMO) radar with colocated transmit and receive antennas will result in a virtual array as the spatial convolution of the transmit and receive elements. The increased degrees of freedom provide superior performance in close targets' discrimination, parameter estimation, and interference rejection [1], [2]. The orthogonal waveforms transmitted by the MIMO radar result in a wide beam with little gain, and consequently the compact MIMO radar is now widely used in short range sensing applications such as driver assistance, traffic monitoring, and industry automation [1]–[3].

For a compact array, there are various sources that cause the array manifold to deviate from its ideal model. For example, the mutual coupling between array antennas, the variation in the transmission lines and RF components in different channels, and the antenna position shifts due to nonidealities [4]. Array calibration to compensate for these imperfections plays a significant role in applications such as beamforming, direction-of-arrival (DOA) estimation, and interference suppression [4]–[6].

A simple way to calibrate the array is to measure the response of each array element to the incident wave emitted by a point source or reflected by a point target in the far-field and on the broadside of the array, which in the ideal case should be the same for all the channels. Hence, the calibration coefficient for each channel could be determined. This method only compensates the phase and gain imbalance of each channel and cannot compensate the mutual coupling between the channels since the calibration matrix is a diagonal one [5]. The coupling coefficient, or inversely interpreted from the electromagnetics perspective, the mutual impedance between different antenna elements, could be determined for a reciprocal array by sequentially activating the array ports once a time and recording the responses at other ports [7]–[12]. This procedure could be simulated by full-wave computation, which needs the detailed knowledge of the array [7], [8], [10], or it could be measured when the array is not packaged [12], [18]. But both the ways are difficult or impractical to be implemented by the users of the array, for whom recalibration is always necessary because of the changed environmental factors such as temperature and aging.

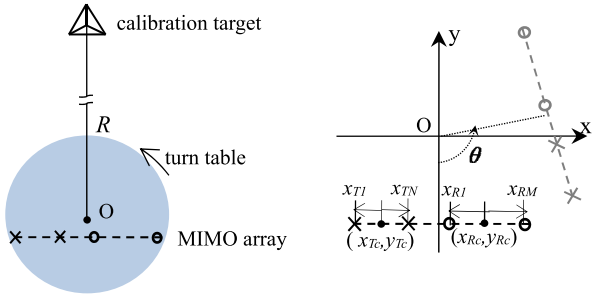

Fig. 1. Geometry for calibration data collection.

In array calibration, the mutual coupling matrix or the calibration matrix can be determined by least-squares fitting of the measured array manifold and the ideal manifold for a few directions [9]–[11], [13]–[16]. In [9], this fitting is presented as Fourier decomposition because the ideal manifold for a uniformly spaced linear array coincides with the basis of Fourier analysis. In [16], the nonisotropic element pattern and the displacement of the array phase center are taken into account in the fitting, with determined models and parameters. For an MIMO array with N transmitters and M receivers, it is always treated as a virtual array with $M \times N$ antennas, and an $M \times N$-by-$M \times N$ calibration matrix is used [3], [17], [19]. But this model violates the fact that mutual coupling only occurs in the physical arrays, which has only $M + N$ elements. What is more, the increased size of the calibration matrix will complicate the process to estimate and implement it in calibration.

In this communication, we propose to calibrate the compact MIMO array using data measured in an anechoic chamber with the radar on a turntable. The calibration model of the MIMO array with an N-by-N matrix to calibrate the transmit array and an M-by-M matrix to calibrate the receive array is proposed with an iterative estimation procedure. The drift of the array from the center of the turntable is included in the calibration model, which greatly facilitates the deployment of data collection. The measurements show that this calibration scheme improves the MIMO array performance in both the angular spectrum of a single target and the superresolution of two closely spaced targets.

II. Signal Model

The geometric arrangement for collecting calibration data is depicted in Fig. 1. The MIMO radar is put on a turntable. The origin of the Cartesian coordinate system coincides with the rotating center. Usually, the center of the MIMO array does not precisely coincide

Manuscript received 7 September 2021; revised 10 February 2022; accepted 20 February 2022. Date of publication 28 March 2022; date of current version 26 July 2022. *(Corresponding author: Zhou Jianxiong.)*

The authors are with the ATR Laboratory, Department of Electronics Science, National University of Defense Technology, Changsha, Hunan 410073, China (e-mail: zjxjanet@sina.com).

Color versions of one or more figures in this communication are available at https://doi.org/10.1109/TAP.2022.3161333.

Digital Object Identifier 10.1109/TAP.2022.3161333

with the rotating center. A calibration target, such as a trihedral, is put in the far-field of the array so that the wavefronts are effectively planar over the array. The target is on the broadside of the array when the rotating angle is zero ($\theta = 0°$).

Taking a linear array into consideration, the location of each transmit antenna is denoted as $\{x_{T1}, \ldots, x_{TN}\}$ with reference to the center of the transmit array, whose coordinate is (x_{Tc}, y_{Tc}). Similar denotations are used for the receive array as $\{x_{R1}, \ldots, x_{RM}\}$ and (x_{Rc}, y_{Rc}). When the turntable rotates with angle θ, the coordinates of the nth transmit antenna and the mth receive antenna are, respectively,

$$\mathbf{p}_{Tn}(\theta) = \left[(x_{Tc}+x_{Tn})\cos\theta - y_{Tc}\sin\theta \quad (x_{Tc}+x_{Tn})\sin\theta + y_{Tc}\cos\theta \right]^T \tag{1a}$$

$$\mathbf{p}_{Rm}(\theta) = \left[(x_{Rc}+x_{Rm})\cos\theta - y_{Rc}\sin\theta \quad (x_{Rc}+x_{Rm})\sin\theta + y_{Rc}\cos\theta \right]^T \tag{1b}$$

where the superscript T denotes the matrix transpose.

Ideally, the complex coefficient of the target echo when illuminated by the nth transmit antenna and received by the mth receive antenna is

$$s_{nm}(\theta) = \exp\left\{ -j\frac{2\pi f_0}{c}\left(2R + (x_{Tc}+x_{Tn})\sin\theta + y_{Tc}\cos\theta + (x_{Rc}+x_{Rm})\sin\theta + y_{Rc}\cos\theta\right)\right\}. \tag{2}$$

Based on planar wave assumption, the phase delay is caused only by the y coordinates in (1). Equation (2) can be rephrased into

$$s_{nm}(\theta) = \exp\left\{-j\frac{4\pi f_0 R}{c}\right\}\exp\left\{-j\frac{2\pi f_0}{c}(x_c\sin\theta + y_c\cos\theta)\right\} \cdot \exp\left\{-j\frac{2\pi f_0}{c}(x_{Tn}+x_{Rm})\sin\theta\right\} \tag{3}$$

where $x_c = x_{Tc} + x_{Rc}$ and $y_c = y_{Tc} + y_{Rc}$ denote the center of the virtual array. Rearrange the data into an N-by-M matrix

$$\mathbf{S}(\theta) = \begin{bmatrix} s_{11}(\theta) & \cdots & s_{1M}(\theta) \\ & \vdots & \\ s_{N1}(\theta) & \cdots & s_{NM}(\theta) \end{bmatrix} = e^{j\phi_0}e^{j\phi(\theta)}\mathbf{A}(\theta) \tag{4}$$

where $\phi_0 = -((4\pi f_0 R)/c)$ is the phase delay induced by R, $\phi(\theta) = -((2\pi f_0)/c)(x_c\sin\theta + y_c\cos\theta)$ is the phase delay induced by the rotation of the aperture center, and $\mathbf{A}(\theta)$ is the ideal steering vector, though rearranged into a matrix, of the MIMO array in the absence of mutual coupling. The element of the steering vector is $a_{nm}(\theta) = \exp\{-j((2\pi f_0)/c)(x_{Tn}+x_{Rm})\sin\theta\}$, and $x_{Tn}+x_{Rm}$ is the equivalent element position of the virtual single-input multiple-output (SIMO) array.

As deduced in [5], [17], [18], and [20], the mutual coupling in the transmit array or in the receive array can be modeled separately. Consequently, the relationship between the measured data and the ideal data can be described as

$$\mathbf{X}(\theta) = \mathbf{C}_T\mathbf{S}(\theta)\mathbf{C}_R + \mathbf{W}(\theta) \tag{5}$$

where $\mathbf{W}(\theta)$ is the noise in the measurements. In (5), the mutual coupling between the transmit channels is accounted for via an N-by-N coupling matrix $\mathbf{C}_T$, whose diagonal elements also present the imbalance among different transmit channels. Similarly, the imperfection of the receive channels is accounted for via an M-by-M coupling matrix $\mathbf{C}_R$. Our task is to estimate $\mathbf{C}_T$ and $\mathbf{C}_R$ based on $\mathbf{X}(\theta)$ measured in the calibration setup, where $\mathbf{S}(\theta)$ is known except for $\{R, x_c, y_c\}$. Then in applications such as beamforming and DOA estimation, the measurements could be calibrated by

$$\hat{\mathbf{S}}(\theta) = \mathbf{C}_T^{-1}\mathbf{X}(\theta)\mathbf{C}_R^{-1} \tag{6}$$

so that the data could be used as if it is consisted of the conventional steering vector as presented in (4).

There are some notes on the mutual coupling model in (5).

1) Only the mutual coupling between either the transmit array elements or the receive array elements is taken into account. Fortunately, the coupling between the transmit and receive array elements is likely minor or negligible given the separation between them. As to the direct wave from the transmitter to the receiver, its time delay is much shorter than the target echo and can be attenuated through range filtering [5].
2) The coupling model is linear and angular-independent, which is true when the array antennas are minimum scatterers with respect to impedance or admittance parameters [7], [11], [20], or when the shape of the current distribution on the stand-alone antenna element is angular-independent [9], [11]. Otherwise, the mutual coupling matrix is viewed as an average of the angular-dependent relationship between the active and the stand-alone array manifold [4], [10], [11], [16]. An angular-dependent calibration model, i.e., $\mathbf{C}(\theta)$ could be used in beamforming where the expected direction of the beam is settled as θ [10], and in DOA searching where each possible direction is tested [21]. However, in angle estimation method such as estimation of signal parameters via rotational invariance techniques (ESPRIT) and root-MUltiple SIgnal Characterization (MUSIC), an angular-dependent calibration will be unrealistic because the direction of the target is unavailable in prior.
3) Ignoring the nonisotropic element pattern and the displacement of the array phase center will lead to a poor match between the measured and ideal data. In [16], these two factors are described by determined models with prior knowledge. From a practical point of view, we treat $\{R, x_c, y_c\}$ as unknowns and estimate them together with the coupling matrix. The energy attenuation caused by the beam pattern is compensated by normalization of the measured data so that $\|\mathbf{X}(\theta)\|_F = \|\mathbf{A}(\theta)\|_F = \sqrt{MN}$ for each θ, where $\|\cdot\|_F$ is the Frobenius norm of a matrix.
4) Equation (5) can be rephrased as

$$\mathbf{x}(\theta) = \mathbf{C}\mathbf{s}(\theta) + \mathbf{w}(\theta) \tag{7}$$

where

$$\mathbf{C} = \mathbf{C}_R^T \otimes \mathbf{C}_T \tag{8}$$

and $\mathbf{x}(\theta)$,$\mathbf{s}(\theta)$,$\mathbf{w}(\theta)$ are the NM-by-1 vectors by stacking the columns of the N-by-M matrices $\mathbf{X}(\theta)$, $\mathbf{S}(\theta)$,$\mathbf{W}(\theta)$ into vectors, and $\otimes$ denotes the Kronecker product. The mutual coupling model in (7) seems identical to that used for a phased array at first glance, but for MIMO array the coupling matrix $\mathbf{C}$ should have particular structure as shown in (8) with less parameters to estimate. Also, the calibration procedure in (6) will be more computationally efficient than by calculating $\mathbf{C}^{-1}\mathbf{x}(\theta)$.

III. Calibration Algorithm

The estimation problem for the parameters in (5) could be rephrased as

$$\left\{\hat{\mathbf{C}}_T, \hat{\mathbf{C}}_R, \hat{R}, \hat{x}_c, \hat{y}_c\right\} = \arg_{\{\mathbf{C}_T, \mathbf{C}_R, R, x_c, y_c\}}\min \sum_{k=1}^{K}\left\|\mathbf{X}(\theta_k) - e^{j\phi_0}e^{j\phi(\theta_k)} \cdot \mathbf{C}_T\mathbf{A}(\theta_k)\mathbf{C}_R\right\|_F^2 \tag{9}$$

where $\{\theta_1, \ldots, \theta_K\}$ is the sampling angle of the turntable, and $\|\cdot\|_F$ is the Frobenius norm of a matrix. The objective in (9) is reasonable for observations in independent additive Gaussian noise. This problem

has two differences from the least-squares solution in [10], [11], and [13]–[16].

1) The inaccuracy of the scene parameters $\{R, x_c, y_c\}$ is taken into consideration. These parameters could be canceled out by selecting a referenced channel, for example, $\mathbf{X}'(\theta) = \mathbf{X}(\theta)/x_{11}(\theta)$ and $\mathbf{S}'(\theta) = \mathbf{S}(\theta)/s_{11}(\theta)$. But the noise in $\mathbf{X}'(\theta)$ will be enlarged and is no longer independent or Gaussian.
2) The coupling matrices for the transmitting array and the receiving array are estimated separately instead of combining them into a coupling matrix $\mathbf{C}$ for the virtual array. If the coupling model is rephrased as in (7), the problem could be solved by a routine least-squares fitting with measurements at different θ. But the solution does not fulfill the constraint in (8), and hence cannot represent the coupling mechanism of an MIMO array. Treating the MIMO array as a virtual SIMO array will improperly enlarge the dimension of the parameter space, which leads to overfitting and hence deteriorates the calibration performance, as will be demonstrated in Section IV.

Based on these two considerations, we keep all the unknowns $\{\mathbf{C}_T, \mathbf{C}_R, R, x_c, y_c\}$ in (9), which is more difficult to solve but has better physical consistence and will provide better calibration performance.

We propose to solve the optimization problem in (9) iteratively. The initial guess for the calibration matrix is $\hat{\mathbf{C}}_{T0} = \mathbf{I}_{N\times N}$ and $\hat{\mathbf{C}}_{R0} = \mathbf{I}_{M\times M}$, and the qth iterative is decomposed into two steps.

Step 1: Estimate $\{R, x_c, y_c\}$ by substituting the previous estimates of $\mathbf{C}_R$ and $\mathbf{C}_T$, i.e., $\hat{\mathbf{C}}_{R(q-1)}$ and $\hat{\mathbf{C}}_{T(q-1)}$ in (9).

In this step, each summation item in (9) could be minimized separately. Denoting $p_k = e^{j\phi_0}e^{j\phi(\theta_k)}$, it could be estimated by

$$\hat{p}_k = \frac{vec\left(\hat{\mathbf{C}}_{T(q-1)}\mathbf{A}(\theta_k)\hat{\mathbf{C}}_{R(q-1)}\right)^H vec\left(\mathbf{X}(\theta_k)\right)}{vec\left(\hat{\mathbf{C}}_{T(q-1)}\mathbf{A}(\theta_k)\hat{\mathbf{C}}_{R(q-1)}\right)^H vec\left(\hat{\mathbf{C}}_{T(q-1)}\mathbf{A}(\theta_k)\hat{\mathbf{C}}_{R(q-1)}\right)} \tag{10}$$

where $vec(\cdot)$ means stacking the columns of a matrix into a vector. Ideally, we should have

$$p_k = \exp\left\{-j\frac{2\pi f_0}{c}\left(2R + x_c\sin\theta_k + y_c\cos\theta_k\right)\right\} \tag{11}$$

Therefore, $\{R, x_c, y_c\}$ could be estimated from the phase of p_k

$$\begin{bmatrix}\hat{\tilde{R}}\\ \hat{x}_c\\ \hat{y}_c\end{bmatrix}_q = \left(\mathbf{H}^T\mathbf{H}\right)^{-1}\mathbf{H}^T\mathbf{p} \tag{12}$$

where

$$\mathbf{H} = \begin{bmatrix}2 & \sin\theta_1 & \cos\theta_1\\ 2 & \sin\theta_2 & \cos\theta_2\\ \vdots & \vdots & \vdots\\ 2 & \sin\theta_K & \cos\theta_K\end{bmatrix}$$

and $\mathbf{p}^T = -(c/(2\pi f_0))unwrap[\angle\hat{p}_1, \angle\hat{p}_2, \cdots \angle\hat{p}_K]$ is the scaled version of the unwrapped phase of $\hat{p}_k$. The samplings of $\{\theta_k\}$ are supposed to be dense enough for unwrapping, which requires

$$\Delta\theta \le \frac{\lambda}{2\cdot\max_k|x_c\cos\theta_k - y_c\sin\theta_k|}. \tag{13}$$

Since the phase history has an initial ambiguity of multiplies of 2π, the estimate of R in (12) will have an ambiguity of multiplies of $\lambda/2$, denoted by $\tilde{R}$.

Step 2: Renew the estimates of $\mathbf{C}_R$ and $\mathbf{C}_T$ according to (9).

We combine the previous estimates of $\{\hat{\tilde{R}}, \hat{x}_c, \hat{y}_c\}_q$ with the ideal steering matrix as

$$\mathbf{S}_q(\theta_k) = \exp\left\{-j\frac{2\pi f_0}{c}\left(2\hat{\tilde{R}} + \hat{x}_c\sin\theta_k + \hat{y}_c\cos\theta_k\right)\right\}\cdot\mathbf{A}(\theta_k). \tag{14}$$

Now (9) simplifies to

$$\left\{\hat{\mathbf{C}}_{Tq}, \hat{\mathbf{C}}_{Rq}\right\} = \arg_{\{\mathbf{C}_T,\mathbf{C}_R\}}\min\sum_{k=1}^{K}\left\|\mathbf{X}(\theta_k) - \mathbf{C}_T\mathbf{S}_q(\theta_k)\mathbf{C}_R\right\|_F^2. \tag{15}$$

However, (15) is still not feasible analytically and we propose to estimate the two calibration matrices sequentially.

1) Estimate $\mathbf{C}_R$ as if $\mathbf{C}_T$ were known

$$\hat{\mathbf{C}}_{Rq} = \arg_{\mathbf{C}_R}\min\sum_{k=1}^{K}\left\|\mathbf{X}(\theta_k) - \hat{\mathbf{C}}_{T(q-1)}\mathbf{S}_q(\theta_k)\mathbf{C}_R\right\|_F^2. \tag{16}$$

The solution is

$$\hat{\mathbf{C}}_{Rq} = \left(\psi^H\psi\right)^{-1}\psi^H\chi \tag{17}$$

where

$$\chi = \begin{bmatrix}\mathbf{X}(\theta_1)\\ \vdots\\ \mathbf{X}(\theta_K)\end{bmatrix}$$

and

$$\psi = \begin{bmatrix}\hat{\mathbf{C}}_{T(q-1)}\mathbf{S}_q(\theta_1)\\ \vdots\\ \hat{\mathbf{C}}_{T(q-1)}\mathbf{S}_q(\theta_K)\end{bmatrix}$$

and the superscript H denotes conjugate transpose.

2) Estimate $\mathbf{C}_T$ as if $\mathbf{C}_R$ were known

$$\hat{\mathbf{C}}_{Tq} = \arg_{\mathbf{C}_T}\min\sum_{k=1}^{K}\left\|\mathbf{X}(\theta_k) - \mathbf{C}_T\mathbf{S}_q(\theta_k)\hat{\mathbf{C}}_{Rq}\right\|_F^2. \tag{18}$$

The solution is

$$\hat{\mathbf{C}}_{Tq} = \chi'\gamma^H\left(\gamma\gamma^H\right)^{-1} \tag{19}$$

where

$$\chi' = \begin{bmatrix}\mathbf{X}(\theta_1) & \cdots & \mathbf{X}(\theta_K)\end{bmatrix}$$

and

$$\gamma = \begin{bmatrix}\mathbf{S}_q(\theta_1)\hat{\mathbf{C}}_{Rq} & \cdots & \mathbf{S}_q(\theta_K)\hat{\mathbf{C}}_{Rq}\end{bmatrix}.$$

Since $\mathbf{C}_R$ and $\mathbf{C}_T$ in (15) can be scaled arbitrarily, their estimates are normalized after each iteration so that the maximum element is 1.

Stop criteria: Step1–step2 iterations could be stopped if

$$\max\left\{\begin{array}{l}\max_{m,n}\left|\dfrac{\hat{\mathbf{C}}_{Tq}(m,n) - \hat{\mathbf{C}}_{T(q-1)}(m,n)}{\hat{\mathbf{C}}_{Tq}(m,n)}\right|,\\ \max_{m,n}\left|\dfrac{\hat{\mathbf{C}}_{Rq}(m,n) - \hat{\mathbf{C}}_{R(q-1)}(m,n)}{\hat{\mathbf{C}}_{Rq}(m,n)}\right|\end{array}\right\} \le \alpha. \tag{20}$$

We set $\alpha = 0.0001$ in the experiments in Section IV. This criterion is quite rigorous because some elements in the calibration matrices are quite small.

In this algorithm, we propose to find the solution of the high-dimensional optimization problem in (9) sequentially and iteratively. Although there is no guarantee for the optimality of the sequential

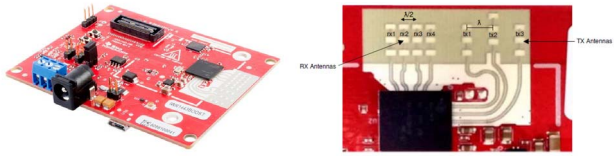

Fig. 2. IWR1443 evaluation module and its MIMO antenna array [22].

solution for the original problem, our experiences show that the convergent results can be reached with good calibration performance. One of the examples will be given in Section IV.

IV. Experiment and Verification

The IWR1443 BoosterPack^{TM} developed by Texas Instruments [22] is used to collect the MIMO array data and test the calibration performance. The evaluation module includes onboard etched microstrip antennas with three transmitters and four receivers, as shown in Fig. 2. In our experiment, only TX1 and TX3 are enabled to form a linear MIMO array with the four receivers.

The module includes an internal processor and hardware architecture to enable self-calibration and monitoring [23]. The inner built RF calibration is carried out for TX or RX channels separately, which compensate for the channel imbalance in phase or gain. The method proposed in this communication is used to further calibrate the array, including the mutual coupling between different channels. The measurement is carried out in an anechoic chamber, and the scene setting is similar to that in Fig. 1. The array is set on a motor-controlled turntable. A trihedral is used as a calibration target and its distance to radar is about 1.1 m, which fulfills the far-field geometry since $2L^2/\lambda = 0.128$m for this MIMO array. The rotate angle θ varies from -40° to 40° with 1° interval. The emitted signal is linear-frequency-modulated with a chirp rate of 2.573×10^{13} Hz/s, and the received signal is dechirped and 64 samplings at the sampling rate of 2 MHz are used to produce the range profile at each azimuth angle. Therefore, the bandwidth is 823 MHz centered at 78.5 GHz. The peaks of the trihedral in the range profiles of each TX–RX combinations are extracted and compiled into the data matrix $\mathbf{X}(\theta_k)$ after normalization, which is a 2-by-4 matrix for each angle θ_k.

The algorithm in Section III is applied and it reaches the stop criteria in (20) after 90 iterations. The estimates of the displacement of the array center are $\hat{x}_c = 9.4$ mm and $\hat{y}_c = -102.2$ mm. The amplitude and phase of the elements in $\hat{\mathbf{C}}_T$ and $\hat{\mathbf{C}}_R$ are as follows:

$$|\hat{\mathbf{C}}_T| = \begin{bmatrix} 0.99 & 0.0263 \\ 0.0199 & 1 \end{bmatrix} \tag{21a}$$

$$\angle\hat{\mathbf{C}}_T = \begin{bmatrix} 0.10 & -0.14 \\ -0.01 & 0 \end{bmatrix} \tag{21b}$$

$$|\hat{\mathbf{C}}_R| = \begin{bmatrix} 0.9219 & 0.0852 & 0.0781 & 0.0814 \\ 0.0712 & 0.8766 & 0.1211 & 0.0789 \\ 0.0784 & 0.1080 & 0.8107 & 0.1458 \\ 0.0640 & 0.0498 & 0.1048 & 1 \end{bmatrix} \tag{22a}$$

$$\angle\hat{\mathbf{C}}_R = \begin{bmatrix} -0.14 & -1.78 & 1.93 & 2.52 \\ 3.08 & 0.12 & -1.74 & -0.41 \\ -0.71 & -1.85 & 0.10 & -3.01 \\ 1.73 & 1.05 & -1.33 & 0 \end{bmatrix}. \tag{22b}$$

The diagonal elements in $\mathbf{C}_T$ and $\mathbf{C}_R$ represent the channel imbalance, which are close to each other since the built-in calibration has been done before data collection. The off-diagonal elements represent the mutual coupling between different channels. The mutual coupling between the receive channels is much higher than that between the transmit channels. This is because the interelement spacing of the receive array is $\lambda/2$, whereas the interelement spacing of the transmit array is 2λ. What is more, the mutual coupling between the adjacent antenna elements is more significant than that between the nonadjacent pairs; therefore, the elements on the first diagonal of $\mathbf{C}_R$ have larger amplitude than those on higher order diagonals in most cases.

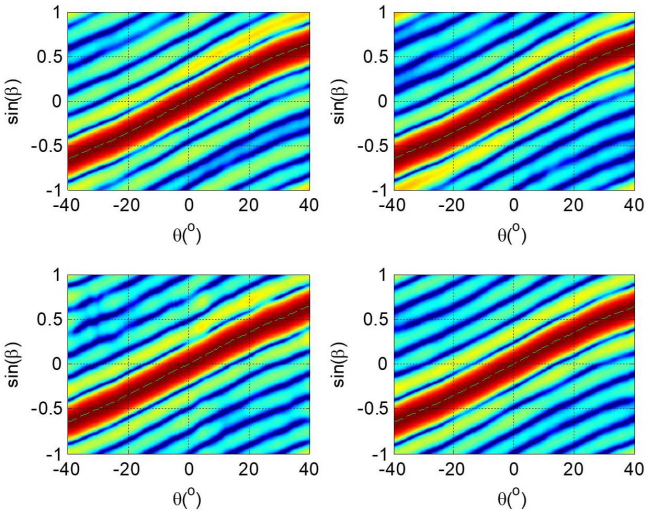

Fig. 3. Angular spectrum at all the azimuth angles by different calibration methods. Original data which have been calibrated by the inner built mechanism of this IWR1443 pack (top left); calibrated by $\theta = 0$ data (top right); calibrated by the SIMO model (bottom left); and calibrated by the MIMO model (bottom right).

First, we check the beam formation and angle estimation performance of different calibration methods. Four different calibration results are compared: 1) self-calibration by IWR1443's internal processor and hardware architectures, i.e., the collected data are used without further calibration; 2) calibration by the data at $\theta = 0^\circ$, i.e., $\hat{s}_{nm}(\theta) = x_{nm}(\theta)/x_{nm}(0)$, $n = 1, \ldots, N, m = 1, \ldots, M$, which further compensates for the interchannel imbalances across all the TX–RX combinations; 3) calibration as if the data were produced by an SIMO array with one transmitter and eight receivers, and the algorithm in Section III is used by setting $\mathbf{C}_T = 1$ and $\mathbf{C}_R$ to be an 8-by-8 matrix; and 4) MIMO calibration by the proposed algorithm with the results shown in (21) and (22).

To verify the applicability of the calibration matrices, we collect the turntable data once more with a trihedral 0.98 m away from the radar, and the sampling interval of the rotate angle is 0.1°. Fig. 3 shows the angular spectrum of the target at all the azimuth angles. Since the virtual aperture is a uniform linear array with eight elements, the angular spectrum is formed by Fourier transform of the data, and the ideal spectrum should have the shape of

$$f(u) = \frac{\sin(8(u - u_0))}{\sin(u - u_0)} \tag{23}$$

and centered at $u_0 = \pi \sin(\theta)$. The shape of the spectrum can be roughly compared from the subfigures and we will give quantitative evaluation later. The green dashed line in each subfigure is the maximum point in the spectrum for each azimuth, and ideally it should coincide with $\theta \sim \sin(\theta)$ and each column should be symmetric about this line. The result by the MIMO calibration (bottom-right subfigure) seems to approach the ideal result most with the evenly arranged sidelobes.

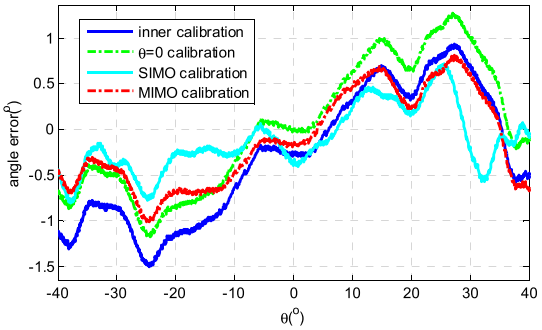

Fig. 4. Azimuth estimation error by different calibration methods.

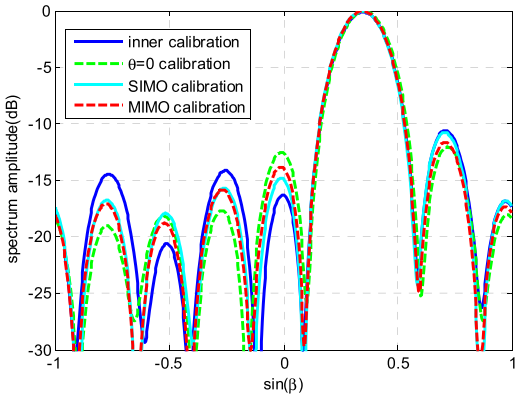

Fig. 5. Angular spectrum of the target at $\theta = 20°$.

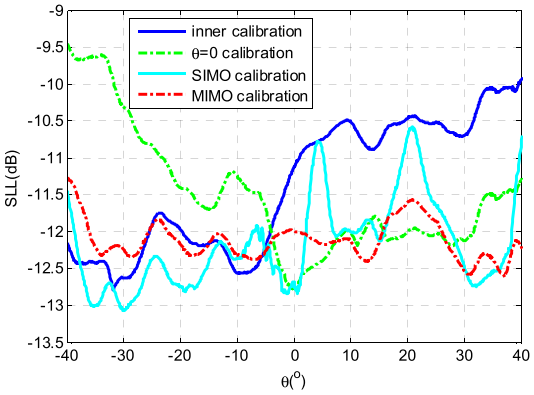

Fig. 6. Maximum SLL at different angles.

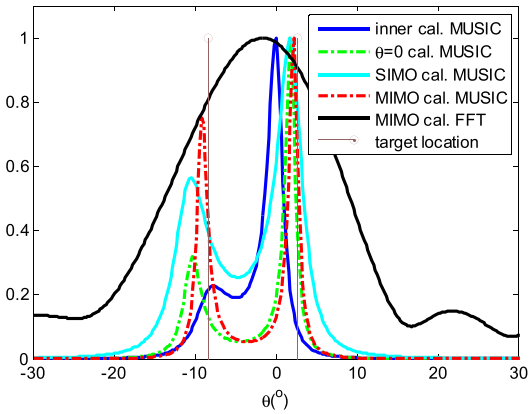

Fig. 7. Spectrum of two closely spaced targets.

The azimuth estimate is obtained from the maximum point in the spectrum, as indicated by the dashed green line in Fig. 3. The estimation error by different calibration methods is shown in Fig. 4. There are small and fast variations due to the discretization of fast Fourier transform (FFT). The angle error of $\theta = 0$ calibration is roughly a shift version of that of the original data, so that the angle error is zero at $\theta = 0°$. The SIMO and MIMO calibration can reduce the error since they compensate for the mutual coupling in the array. The SIMO calibration presents smaller error than MIMO calibration. This is reasonable because the SIMO calibration matrix is of size 8×8 with 64 parameters, whereas MIMO calibration matrices are of sizes 2×2 and 4×4, with only 20 parameters. This implies that SIMO calibration is more apt to be overfitted, which will lead to a more fluctuant spectrum, as can be observed in the bottom-left subfigure in Fig. 3 and will be evaluated quantitatively in the following.

Fig. 5 shows the angular spectrum at $\theta = 20°$. The maximum sidelobe level (SLL) is -10.5, -12, -10.7, and -11.6 dB for the four results, respectively. Ideally, the maximum SLL for (23) should be -12.8 dB, whereas the mutual coupling among the channels distorts the spectrum and increases the SLL. After calibration, the sidelobes are more regular. In this single case, MIMO calibration outperforms SIMO calibration but does not provide the SLL closest to the ideal value. The maximum SLLs at all the angles are plotted in Fig. 6. We see that the MIMO calibration provides consistent performance in the whole azimuth scope to produce maximum SLL close to -12.8 dB, whereas other methods may have lower SLL at some angles and much higher SLL at others. MIMO calibration outperforms others because its model is better with the mutual coupling mechanism in an MIMO array, and therefore it can correct the beam distortion induced by mutual coupling better.

Next, we inspect the spectrum of two closely spaced targets and show how the calibration benefits the superresolution algorithm. Two trihedrals are put at the same distance (R $\approx$ 1.1 m) with cross-range spacing of about 21 cm. The azimuth interval is about 11° which is beneath the Rayleigh resolution limit. The MUSIC algorithm with spatial smoothing [24] is used to achieve superresolution. The subspace-based superresolution algorithm is more sensitive to coupling error than the Fourier transform because it explores the prior knowledge of the ideal steering vector via nonlinear processing. So a careful calibration is important for successful operation of the superresolution techniques [9], [13], [21]. Fig. 7 shows the MUSIC spectrum after calibration by different methods. As a comparison, the Fourier spectrum after MIMO calibration is also shown. The two targets are merged into one peak in the Fourier spectrum, whereas they can be resolved in the MUSIC spectrum. What is more, the MUSIC spectrum after MIMO calibration has much better resolving performance than other calibration methods, which verifies the effectiveness of the MIMO calibration method in correcting the data to the ideal signal subspace of an MIMO array.

V. Conclusion

In this communication, we propose a compact MIMO radar calibration method which has three dominant features.

1) The calibration data are collected by putting the radar on a turntable and illuminating a point target. The position drift of the array from the center of the turntable could be estimated together with the calibration matrices, and this facilitates the measurement setup.

2) Both the mutual coupling and the channel imbalances could be compensated, which is especially helpful to compact array with closely spaced antennas.
3) The mutual coupling between the transmit channels or between the receive channels is compensated separately, which consists of the coupling mechanism of the MIMO array and has better calibration performance in beamforming, angle estimation, and close targets' superresolution. In addition, treating the transmit and receive array separately needs much less parameters than treating them as a virtual SIMO array, which also reduces the computation load of calibration.

Further researches should include: 1) the modification of the calibration algorithm when planar wave assumption is not fulfilled, for example, a large sparse array in a small anechoic chamber, and 2) the calibration of a 2-D planar array with a turntable which can rotate in both azimuth and elevation.

REFERENCES

[1] J. Li and P. Stoica, "MIMO radar with colocated antennas," *IEEE Signal Process. Mag.*, vol. 24, no. 5, pp. 106–114, Sep. 2007.

[2] S. Sun, A. P. Petropulu, and H. V. Poor, "MIMO radar for advanced driver-assistance systems and autonomous driving: Advantages and challenges," *IEEE Signal Process. Mag.*, vol. 37, no. 4, pp. 98–117, Jul. 2020.

[3] C. Vasanelli, R. Batra, A. D. Serio, F. Boegelsack, and C. Waldschmidt, "Assessment of a millimeter-wave antenna system for MIMO radar applications," *IEEE Antennas Wireless Propag. Lett.*, vol. 16, pp. 1261–1264, 2017.

[4] C. M. Schmid, S. Schuster, R. Feger, and A. Stelzer, "On the effects of calibration errors and mutual coupling on the beam pattern of an antenna array," *IEEE Trans. Antennas Propag.*, vol. 61, no. 8, pp. 4063–4072, Aug. 2013.

[5] B. T. Arnold and M. A. Jensen, "The effect of antenna mutual coupling on MIMO radar system performance," *IEEE Trans. Antennas Propag.*, vol. 67, no. 3, pp. 1410–1416, Mar. 2019.

[6] H. Singh, H. L. Sneha, and R. M. Jha, "Mutual coupling in phased arrays: A review," *Int. J. Antennas Propag.*, vol. 2013, pp. 1–23, Mar. 2013.

[7] I. J. Gupta and A. A. Ksienski, "Effect of mutual coupling on the performance of adaptive arrays," *IEEE Trans. Antennas Propag.*, vol. AP-31, no. 5, pp. 785–791, Sep. 1983.

[8] H. T. Hui, "Improved compensation for the mutual coupling effect in a dipole array for direction finding," *IEEE Trans. Antennas Propag.*, vol. 51, no. 9, pp. 2498–2503, Sep. 2003.

[9] H. Steyskal and J. S. Herd, "Mutual coupling compensation in small array antennas," *IEEE Trans. Antennas Propag.*, vol. 38, no. 12, pp. 1971–1975, Dec. 1990.

[10] K. R. Dandekar, H. Ling, and G. Xu, "Experimental study of mutual coupling compensation in smart antenna applications," *IEEE Trans. Wireless Commun.*, vol. 1, no. 3, pp. 480–487, Jul. 2002.

[11] T. Su and H. Ling, "On modeling mutual coupling in antenna arrays using the coupling matrix," *Microw. Opt. Technol. Lett.*, vol. 28, no. 4, pp. 231–237, Feb. 2001.

[12] A. H. Mohammadian, N. M. Martin, and D. W. Griffin, "A theoretical and experimental study of mutual coupling in microstrip antenna arrays," *IEEE Trans. Antennas Propag.*, vol. 37, no. 10, pp. 1217–1223, Oct. 1989.

[13] A. N. Lemma, E. F. Deprettere, and A.-J. van der Veen, "Experimental analysis of antenna coupling for high-resolution DOA estimation algorithms," in *Proc. 2nd IEEE Workshop Signal Process. Adv. Wireless Commun.*, Jul. 1999, pp. 362–365.

[14] E. K. L. Hung, "Matrix-construction calibration method for antenna arrays," *IEEE Trans. Aerosp. Electron. Syst.*, vol. 36, no. 3, pp. 819–828, Jul. 2000.

[15] I. J. Gupta, J. R. Baxter, S. W. Ellingson, H.-G. Park, O. H. Seo, and K. M. Geon, "An experimental study of antenna array calibration," *IEEE Trans. Antennas Propag.*, vol. 51, no. 3, pp. 664–667, Mar. 2003.

[16] B. Lindmark, "Comparison of mutual coupling compensation to dummy columns in adaptive antenna systems," *IEEE Trans. Antennas Propag.*, vol. 53, no. 4, pp. 1332–1336, Apr. 2005.

[17] A. Durr *et al.*, "On the calibration of mm-Wave MIMO radars using sparse antenna arrays for DoA estimation," in *Proc. 49th Eur. Microw. Conf. (EuMC)*, Paris, France, Oct. 2019, pp. 349–352.

[18] G. Babur, P. J. Aubry, and F. Le Chevalier, "Antenna coupling effects for space-time radar waveforms: Analysis and calibration," *IEEE Trans. Antennas Propag.*, vol. 62, no. 5, pp. 2572–2586, May 2014.

[19] R. L. Grove and J. Dall, "On the impact of channel imbalance on MIMO radar performance," in *Proc. 17th Eur. Radar Conf. (EuRAD)*, Jan. 2021, pp. 330–333.

[20] B. Clerckx *et al.*, "Impact of antenna coupling on 2×2 MIMO communications," *IEEE Trans. Veh. Technol.*, vol. 56, no. 3, pp. 1009–1018, May 2007.

[21] Q. Yuan, Q. Chen, and K. Sawaya, "Accurate DOA estimation using array antenna with arbitrary geometry," *IEEE Trans. Antennas Propag.*, vol. 53, no. 4, pp. 1352–1357, Apr. 2005.

[22] *IWR1443 Evaluation Module (IWR1443BOOST) mmWave Sensing Solution User's Guide*. Accessed: Dec. 2018. [Online]. Available:https://www.ti.com/tool/IWR1443BOOST

[23] *Self-Calibration in TI's mmWave Radar Devices*. Accessed: Jan. 2021. [Online]. Available: https://www.ti.com/lit/pdf/spracf4

[24] T.-J. Shan, M. Wax, and T. Kailath, "On spatial smoothing for direction-of-arrival estimation of coherent signals," *IEEE Trans. Acoust., Speech, Signal Process.*, vol. ASSP-33, no. 4, pp. 806–811, Aug. 1985.